Scaling of the power exhaust channel in Alcator C-Mod

Cite as: Phys. Plasmas **18**, 056104 (2011); https://doi.org/10.1063/1.3566059
Submitted: 19 November 2010 . Accepted: 24 January 2011 . Published Online: 22 April 2011

B. LaBombard, J. L. Terry, J. W. Hughes, D. Brunner, J. Payne, M. L. Reinke, I. Cziegler, R. Granetz, M. Greenwald, I. H. Hutchinson, J. Irby, Y. Lin, B. Lipschultz, Y. Ma, E. S. Marmar, W. L. Rowan, N. Tsujii, G. Wallace, D. G. Whyte, S. Wolfe, S. Wukitch, G. Wurden, and Alcator C-Mod Team

Scaling of the power exhaust channel in Alcator C-Mod[a)]

B. LaBombard,[1,b)] J. L. Terry,[1] J. W. Hughes,[1] D. Brunner,[1] J. Payne,[1] M. L. Reinke,[1] I. Cziegler,[1] R. Granetz,[1] M. Greenwald,[1] I. H. Hutchinson,[1] J. Irby,[1] Y. Lin,[1] B. Lipschultz,[1] Y. Ma,[1] E. S. Marmar,[1] W. L. Rowan,[2] N. Tsujii,[1] G. Wallace,[1] D. G. Whyte,[1] S. Wolfe,[1] S. Wukitch,[1] G. Wurden,[3] and Alcator C-Mod Team[1]
[1]*MIT Plasma Science and Fusion Center, Cambridge, Massachusetts 02139, USA*
[2]*University of Texas, Fusion Research Center, Austin, Texas 78712, USA*
[3]*Los Alamos National Laboratory, Los Alamos, New Mexico 87545, USA*

(Received 19 November 2010; accepted 24 January 2011; published online 22 April 2011)

Parametric dependences of the heat flux footprint on the outer divertor target plate are explored in EDA H-mode and ohmic L-mode plasmas over a wide range of parameters with attached plasma conditions. Heat flux profile shapes are found to be independent of toroidal field strength, independent of power flow along magnetic field lines and insensitive to x-point topology (single-null versus double-null). The magnitudes and widths closely follow that of the "upstream" pressure profile, which are correlated to plasma thermal energy content and plasma current. Heat flux decay lengths near the strike-point in H- and L-mode plasmas scale approximately with the inverse of plasma current, with a diminished dependence at high collisionality in L-mode. Consistent with previous studies, pressure gradients in the boundary scale with plasma current squared, holding the magnetohydrodynamic ballooning parameter approximately invariant at fixed collisionality—strong evidence that critical-gradient transport physics plays a key role in setting the power exhaust channel. © *2011 American Institute of Physics*. [doi:10.1063/1.3566059]

I. INTRODUCTION

The width of power exhaust channel at the divertor plate, λ_q, is a critical engineering parameter for any tokamak with reactor-level power entering into its scrape-off layer (P_{SOL}). Yet, physics-based transport models that can accurately simulate observed λ_q values and their scalings in existing tokamaks are lacking at the present time.

The maximum steady-state heat flux that can be safely handled by a material surface is typically ~10 MW m^{-2}, the value which is presently set for ITER's (international thermonuclear experimental reactor) peak divertor heat fluxes.[1] Because of this constraint, the size of λ_q directly sets the acceptable fraction of P_{SOL} that may impinge divertor surfaces, $f_{div}P_{SOL}$. For ITER, f_{div} is estimated to be $f_{div} < \sim 0.04\lambda_q$,[2] with λ_q expressed in millimeters, magnetically mapped to the outboard midplane. Thus ~5 mm λ_q value, currently projected for ITER, mandates that ~80% of P_{SOL} must be dissipated to avoid damage to divertor surfaces and associated coolant structures. This in turn demands that ITER must be operated in a partially detached divertor regime—a regime that is not guaranteed to be compatible with the desired core plasma performance ($Q_{DT} \sim 10$). The situation expected for a DEMO is even more severe, having several times ITER's P_{SOL} in a device of similar size.[3] However, the ~5 mm value for ITER is based in part on empirical projections from present day experiments,[2,4,5] which appear to be ambiguous and not well formulated. Of primary concern are the inconsistencies with respect to major radius (R), scrape-off layer power (P_{SOL}) or divertor power (P_{div}), and engineering parameters such as toroidal magnetic field (B_ϕ) and plasma current (I_p), or safety factor (q_{95}).

Multimachine scalings based on heat flux "footprints" measured at the outer divertor surface of ELMy H-modes[4] suggested very weak or no scaling with machine size, a positive power-law dependence on P_{SOL} ($\sim P_{TOT} \sim P_{div}$) and a sensitivity to B_ϕ and q_{95}. Power-law regression analyses yielded the expressions

$$\lambda_q^{H-1}(m) = (5.2\pm1.3)10^{-3} P(MW)_{div}^{0.44\pm0.04} \times B(T)_\phi^{-0.45\pm0.07} q_{95}^{0.57\pm0.16}, \quad (1)$$

$$\lambda_q^{H-2}(m) = (5.3\pm1.4)10^{-3} P(MW)_{TOT}^{0.38\pm0.04} \times B(T)_\phi^{-0.71\pm0.08} q_{95}^{0.30\pm0.15}. \quad (2)$$

Yet, multimachine scaling studies of the temperature e-folding lengths at the last-closed flux surface (LCFS) near the outer midplane[6,7] revealed that major radius is the dominant scale parameter. This observation appears to be inconsistent with the above scalings, given that the upstream electron temperature profile is thought to play such a dominant role in setting the width of the power exhaust channel. Adding to these ambiguities, detailed analyses of the power exhaust channel in JET identified a different set of empirical scaling projections for λ_q,[5]

$$\lambda_q^{cond} \propto B_\phi^{-1} P_{SOL}^{-0.5} n_{e,u}^{0.25} q_{95} R^2 \text{ (conduction limited case)}, \quad (3)$$

$$\lambda_q^{conv} \propto B_\phi^{-1} P_{SOL}^{-0.5} n_{e,u}^{0.25} q_{95}^{0.5} R^{1.5} \text{ (sheath-limited case)}, \quad (4)$$

which includes upstream electron density, $n_{e,u}$, as a parameter. This scaling contains a negative power-law sensitivity to P_{SOL}, an inverse scaling with B_ϕ and a major radius

[a)]Paper JI2 4, Bull. Am. Phys. Soc. **55**, 149 (2010).
[b)]Invited speaker.

proportionality, combined with a linear or square-root sensitivity to the field line connection length in the scrape-off layer, $q_{95}R$, depending on the parallel heat transport regime. This ambiguous state of affairs has existed for some time, as it is plainly stated in the 2007 ITER Physics basis document:[2] "…there is a need for improved experimental measurements and a theory-oriented approach for making extrapolations for the target heat flux in ITER…' "

Recognizing these critical gaps in understanding, Alcator C-Mod initiated an aggressive experimental program in 2009 to help contribute to this important science area, first by developing an extensive array of divertor heat flux instrumentation and second by performing dedicated experiments to explore boundary layer heat transport. This paper reports on experiments performed during the FY2010 run campaign, which were part of a coordinated research program with NSTX and DIII-D, in support of a Joint Research Target established by the US DoE Office of Fusion Energy Sciences.[8]

The C-Mod experiments were designed to address specific physics questions: First, what are the typical values of λ_q observed in C-Mod's EDA H-mode and L-mode plasmas? What are the dominant empirical dependencies of λ_q with regard to P_{SOL}, B_ϕ, I_p, and parallel connection length? How does the outer divertor heat flux footprint relate to the plasma parameters observed upstream in the boundary layer plasma? And lastly, how do the observed divertor heat flux profiles connect to previous experimental results reported from C-Mod, which identified critical-gradient transport physics as playing a prominent role in establishing its boundary layer profiles?[9,10] Since this paper focuses on C-Mod's results alone, the issue of major radius scaling is not addressed directly. However, as discussed below, C-Mod's heat flux footprints are found to be connected to the upstream plasma pressure profiles and the behaviors of the H-mode pedestal. This result by itself suggests that λ_q scales with major radius for standard aspect ratio tokamaks, since that is the dominant scale parameter found for upstream electron temperature profiles[6] and pressure gradient widths of H-mode pedestals.[11–13]

Section II discusses in some detail the new divertor diagnostic package developed for these experiments and the methods used to measure footprints. The experiments involving EDA H-modes are introduced in Sec. III, including some of the first heat flux footprint observations obtained in C-Mod. A typical footprint is composed of a "narrow heat flux channel" near the strike-point region (~2 mm wide) and a "tail" feature that extends into the far scrape-off layer (SOL). Contrary to the empirical scalings described above, the heat flux profile is found to be robustly independent of power flow through the SOL. Instead, it is clearly tied to the upstream plasma pressure profile and overall plasma confinement. For EDA H-modes with the highest stored energy, the e-folding widths of the narrow heat flux channel in the common flux region are found to scale as $\sim 1/I_p$, with no dependence on toroidal magnetic field. These results indicate that λ_q is independent of q_{95} at fixed current, or equivalently, field line connection length from "good" to "bad" curvature regions inside the LCFS. The topic of field line connection length *outside* the LCFS is addressed in Sec. IV. There we describe experiments in which magnetic topology was changed dynamically from lower single-null (LSN) to double-null (DN), effectively cutting SOL field line lengths in half. Heat flux profile shapes are found to be invariant. These results are consistent with the previous SOL observations and the idea that interchange-driven transport dynamics in the low-field side SOL sets the boundary layer profiles. Section V reports on ohmic L-mode discharges. Here, divertor and upstream plasma conditions are mapped out in detail over wide parameter variation. Again, clear connections are observed between the divertor heat flux profile and pressure profiles upstream. For plasmas with the same line-averaged density normalized to Greenwald density,[14] $\bar{n}_e/n_G$ (or equivalently the same parallel collisionality), upstream pressure profiles and divertor heat flux profiles are unchanged, despite a factor of two change in B_ϕ. Electron pressure gradients, normalized according to the magnetohydrodynamic (MHD) ballooning parameter, α_{mhd} ($\sim 4\mu_0 q_{95}^2 R\,|\nabla n T_e|/B^2$ in mks units), are also found to be invariant and remain approximately so as the plasma current is changed by a factor of 2. These data are found to reproduce and extend previous observations of critical-gradient phenomenology in the C-Mod boundary layer. Finally, λ_q and corresponding upstream pressure gradient lengths are found to scale as $\sim 1/I_p$ in low parallel collisionality conditions (or equivalently, $\bar{n}_e/n_G \lesssim 0.2$), revealing an interesting commonality in boundary layer transport behaviors among H- and L-mode plasmas.

II. EXPERIMENTAL ARRANGEMENT

A. Divertor heat flux diagnostics

The results from boundary layer heat transport experiments reported in this paper were made possible by the installation of a new divertor diagnostic package in C-Mod, specifically designed to record thermal loads and plasma parameters across the outer divertor strike-point region.[15–17] Two different installations were performed (2009 and 2010). As shown in Fig. 1, a set of "ramped tiles" was installed in one of C-Mod's outer divertor cassettes, spanning four vertical columns of tiles—approximately 12° of toroidal circumference (2010 installation). The three right-most columns are tilted in the toroidal direction by ~2° and "ramped up" relative to standard tiles, starting from a location that is 1 mm recessed below the standard tile surface and ending at a location that is 2 mm extended above. Thus, the far right column is purposefully shadowed by adjacent tiles, providing a means to subtract background light in the IR camera view. The final, left-most column maintains the 2 mm extension for one tile width. This arrangement ensures that field lines striking the leftmost columns will not be shadowed by adjacent divertor cassette and/or tile misalignments—a situation that is regularly seen elsewhere on C-Mod's vertical target face where a typical field line grazing angle is under 1°. This ramped-tile arrangement also increases the incident heat flux density, enhancing the signal-to-noise ratio of thermal diagnostics. The diagnostic package includes an extensive array of embedded calorimeters (13), tile thermocouples (10),

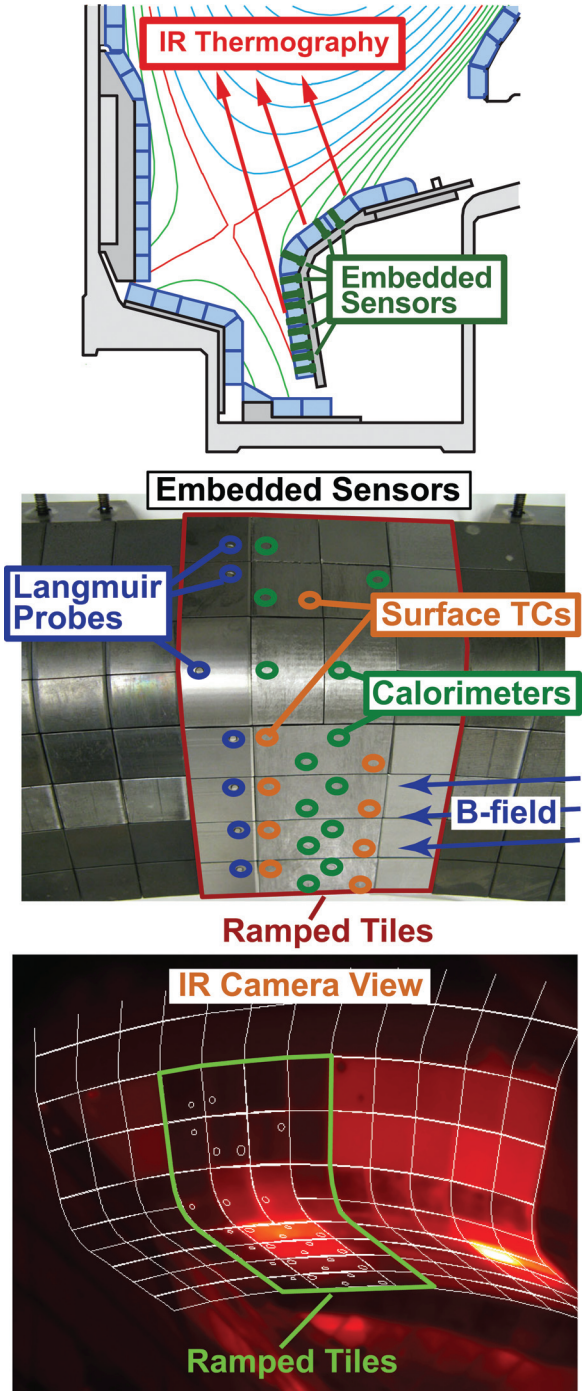

FIG. 1. (Color online) In order to facilitate measurements of divertor heat flux "footprints" in Alcator C-Mod, a set of "ramped tiles" was installed in one of the outer divertor cassettes and instrumented with an extensive array of embedded thermal sensors and Langmuir probes (hardware from 2010 installation is shown). An IR camera system was assembled to view the ramped-tile surfaces from above at oblique angles (Refs. 16, 19).

surface thermocouples (9), Langmuir probes (LPs) (7), and an IR periscope[18] coupled to a FLIR SC7000 camera. The diagnostic/tile arrangement for the earlier installation (2009) was similar to that shown in Fig. 1, except that it included only the two central tile columns and no embedded LPs. In this case, an older LP array, embedded in a standard divertor cassette located 90° away toroidally, was used to characterize the divertor conditions. However, subsequent cross-comparisons between the old and new LP arrays revealed that some of the old LPs can be corrupted by shadowing effects and therefore their data must be treated with caution. The EDA H-mode data reported in this paper (Sec. III) were obtained using the 2009 installation. Data from x-point balance experiments and ohmic L-modes (Secs. IV and V) were obtained from the 2010 diagnostic package (Fig. 1).

The IR camera detects emission in a 3–5 μm range with 320×256 pixel resolution.[19] It views the ramped tiles by looking both down and in the toroidal direction from a periscope in a vertical port ($\sim$90° away toroidally), such that it can view the otherwise hidden vertical segment of the tile surface. A reference image used for camera alignment is shown in Fig. 1. IR thermography is particularly challenging in C-Mod with its shiny, low emissivity, molybdenum tile surfaces, and oblique observations angles[16,19]—an environment that is similar to ITER. These complexities are handled by *in-situ* IR calibrations and by performing various cross-checks with embedded sensors. Additional complications include low-Z surface films (e.g., boron) that change in time and image movement due to relative machine/periscope/camera motion that routinely exceeds 20 pixels in the image. To compensate for the image movement, the overall tile pattern seen in Fig. 1 is used as a landmark to numerically stabilize the image, necessitating the wide field-of-view. Nevertheless, the camera/periscope system resolves $\sim$1 mm scale features on the ramped-tile surfaces.

A two-dimensional (2D) thermal model of the ramped-tile section (QFLUX_2D) is used to convert the surface temperature measurements to surface heat fluxes. QFLUX_2D contains a dimensionally accurate 2D description of C-Mod's ramped-tile geometry, including tile gaps (see Fig. 2), at a cross-section corresponding to the ramped tile's midsection in toroidal angle. Since the ramped tiles are also segmented in the toroidal direction, heat flow in that direction is small and therefore neglected. QFLUX_2D accounts for temperature-dependent materials properties and allows a thermal resistance layer (film) profile to be specified. Surface films can change the relationship between surface temperature and heat flux and, if not properly considered, can lead to erroneous negative heat fluxes.[20] We employ a novel Fourier analysis method to estimate the thermal resistance of films: (1) computing the complex thermal impedance of a bare surface using measured temperatures and modeled heat fluxes and (2) adding to this a minimal amount of surface thermal resistance to eliminate negative heat fluxes. Figure 2 shows an example of a QFLUX_2D simulation, including surface film compensation (expressed in terms of an equivalent layer of pure boron). It should be noted that without film compensation, transient negative heat fluxes on the order of 20% of the time-averaged value can be seen as power to the divertor is modulated by strike-point sweeps (Sec. IV) or changes in confinement regime (Sec. III). During the discharge (top panel), QFLUX_2D imposes the IR-measured surface temperatures as a time-dependent boundary condition and computes the implied surface heat flux profiles. Peak surface heat fluxes exceeding 10 MW m^{-2}, corresponding to parallel heat fluxes exceeding 200 MW m^{-2}, are routinely observed. Surface thermocouple temperature measurements (seen as blue

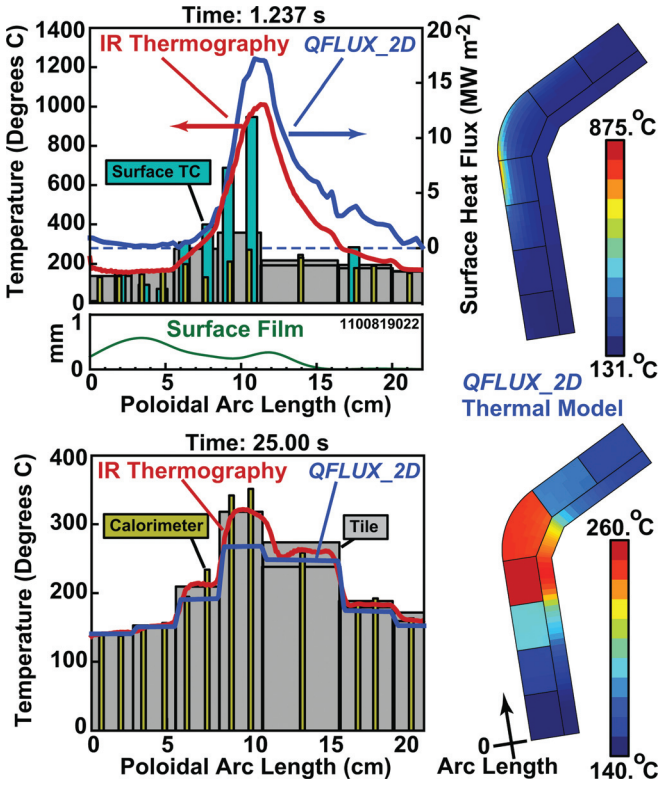

FIG. 2. (Color online) Heat flux profiles during a plasma discharge (top panels) are deduced from surface temperatures using a thermal analysis code, QFLUX_2D. Surface thermocouple data yield valuable cross-checks on IR measurements. At long times after a discharge (bottom panels), calorimeter and tile temperatures are used to calibrate the IR system and to check the overall consistency of the thermal model.

bars in online version of Fig. 2) are found to agree with IR-inferred surface temperature measurements, lending confidence to the data.

Immediately after the discharge, the surface heat flux is set to zero and the modeled temperatures are allowed to evolve, arriving at a tile temperature distribution that can be checked with measurements for overall consistency (lower panel of Fig. 2). At this point in time, an *in-situ* calibration of the IR system is performed, using the tile thermocouple data (seen as gray bars in online version of Fig. 2). This procedure is performed after every discharge to compensate for changes in surface emissivity owing to film evolution and for degradations in periscope transmission.[19]

B. Experimental program

Armed with these new heat flux diagnostics, we performed three separate experimental investigations of footprints in C-Mod: (1) EDA H-modes, (2) influence of magnetic x-point balance, and (3) ohmic L-modes. The primary goals were to unfold the parametric dependencies of C-Mod's heat flux footprints and, if possible, connect the footprint observations (magnitudes, profile widths) to the plasma parameters measured upstream in the boundary layer. However, divertor heat flux profiles and their connection to upstream plasma conditions can be dramatically altered as a divertor transitions from high-recycling to detached regimes; divertor radiation can compete with power flow and momentum losses can affect pressure balance. We therefore restricted our investigations to discharges in which the outer divertor was fully attached ($T_e > 8$ eV) and the total power incident on the outer divertor was greater than 30% of the power entering into the SOL.

In the highest power discharges (EDA H-modes and x-point balance experiments) the primary diagnostics for the study were IR thermography (spot-checked by embedded sensors) combined with edge Thomson scattering[21] to record the upstream plasma conditions. In the relatively low-power ohmic L-mode experiments, where reduced surface temperature rises render the IR camera less reliable, the heat flux profile was mapped out in detail via embedded Langmuir probes (cross-checked against surface thermocouple sensors). This was accomplished by sweeping the strike-point across the sensors under otherwise constant plasma conditions. Upstream plasma conditions were interrogated in detail by multiple plunges of C-Mod's horizontal scanning probe,[22] which was upgraded in 2008 to an advanced head design for high heat-flux handling.[23,24]

III. EDA H-MODES

EDA H-modes are the first subject of our investigation. These are steady-state discharges in which the pedestal is regulated by a continuous "quasicoherent" edge mode (QCM), rather than by a regular procession of ELMs.[25] We targeted plasmas with varying plasma currents ($I_p = 0.5$, 0.8, 0.9, 1.0 MA), toroidal magnetic fields ($B_T = 4.5$, 5.4, 6.2 T), and ICRF input powers ($P_{\mathrm{ICRF}} = 1$–4.5 MW) in a standard lower-single-null configuration ($\kappa \sim 1.6$, $\delta_L \sim 0.48$, $\delta_U \sim 0.32$). Normalized plasma densities where held to a narrow range ($0.45 < \bar{n}_e/n_G < 0.6$) in which steady EDA H-modes are observed.

A. Heat flux footprints: narrow power channel with a tail

Figure 3 shows a representative 0.9 MA, 5.4 T EDA H-mode discharge, with $P_{\mathrm{ICRF}} = 4$ MW (80 MHz, second-harmonic, hydrogen-minority). Radiated power from the confined plasma (P_{RAD}) is deduced from a resistive bolometer system,[26] providing an estimate of P_{SOL}. Power onto the outer divertor (P_{ODIV}) is computed from the IR-inferred divertor heat flux profiles. Heat flux footprints are found to exhibit a two zone structure: a narrow "power channel" near the separatrix of ~2 mm wide (characterized by its full-width at half-maximum, FWHM, mapped to the outer midplane), and a tail that extends into the far SOL region. It should be noted that the exact location of the separatrix relative to the narrow heat flux channel is uncertain, with shot-to-shot variation on the order of ~1 mm and systematic offsets on the same order. Also shown in Fig. 3 are parallel heat fluxes estimated from Langmuir probes. These data initially verified that the tail feature was real and not some artifact of the IR-inferred heat flux profile. More extensive cross-comparisons have since been performed among IR, LP, and embedded thermal sensors.[27,28] These data verify the full set of IR-inferred heat flux footprints from EDA H-modes reported here.

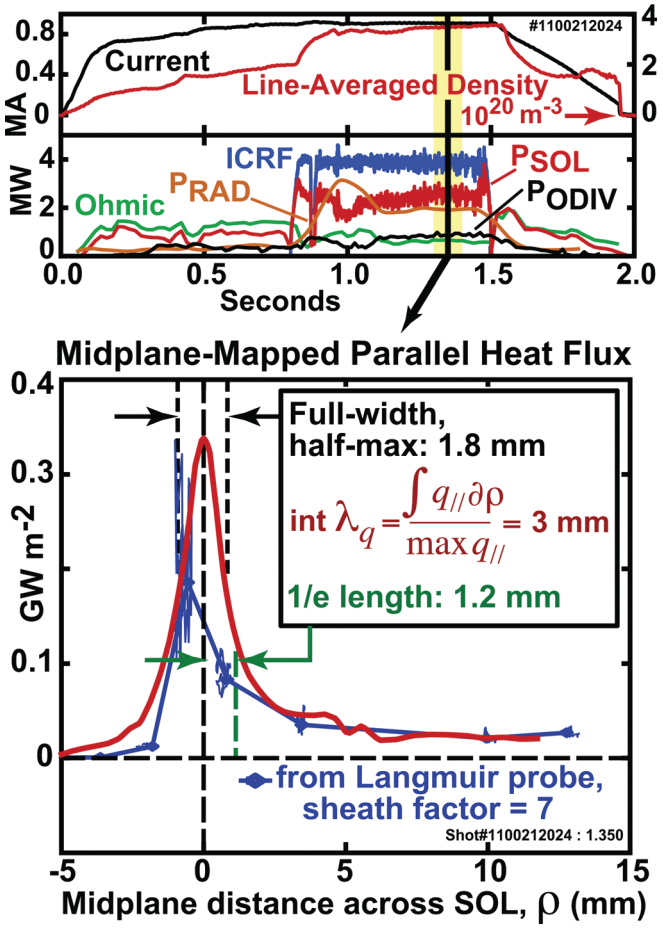

FIG. 3. (Color online) Representative time traces (top panels) and a corresponding divertor heat flux footprint from a steady EDA H-mode discharge. Heat flux profiles from IR camera (red online color, bottom panel) and Langmuir probe array (blue online color) are shown, mapped to the outer midplane. Parallel heat flux profile widths are characterized by the three different measures shown. (Note: Langmuir probe measurements near the strike-point may be partially shadowed by divertor misalignments in this discharge.)

Following the definition of Loarte,[4] the integral heat flux width (integral λ_q) is found to be in the range of ~3 mm for this discharge. Although the tail feature affects this definition, the integration is nonetheless performed over the full profile, from −5 to 15 mm mapped to the outer midplane. Two other measures are also used to track the heat channel width: the full-width at half maximum (FWHM) and the e-folding length (1/e length) in the common flux zone of the narrow heat flux channel (see Fig. 3). It should be noted that empirical scaling laws [e.g., Eqs. (1)–(4)] are generally cast in terms of integral λ_q. However, as discussed below, it is important to track separately the heat flux widths in the near SOL (FWHM, e-folding width) since this region is found to scale differently in some cases.

Turning to the empirical scaling laws, we find that Eq. (1) predicts $\lambda_q \approx 5$ mm while Eq. (3) predicts $\lambda_q \approx 0.7$mm (scaled from JET) for the C-Mod discharge shown in Fig. 3, yet neither of these values is observed. This disappointing result is not surprising, given the complexity of SOL transport physics and the fact that these laws were assembled in the absence of any C-Mod data. In any case, this observation serves as additional motivation for the experimental investigation reported here.

B. Time-dependent observations: λ_q and $q_{//}$

EDA H-modes often exhibit a slow time evolution in boundary layer power flow, as ICRF input power is varied and/or the level of core radiated power changes, owing to the variation in core density and intrinsic impurity concentrations. These cases allow relationships between λ_q and $q_{//}$ to be explored. An example of a 1.0 MA, 5.4 T EDA H-mode discharge is shown in Fig. 4. This plasma exhibited two

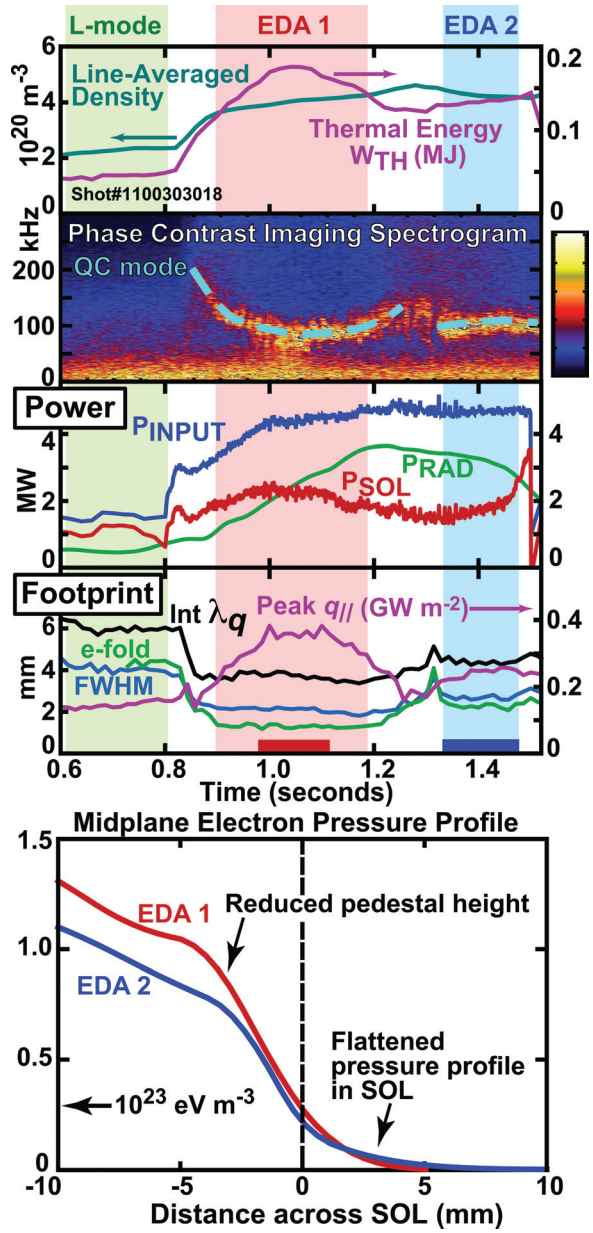

FIG. 4. (Color online) H-mode discharge exhibiting two different time-evolving EDA phases. Peak parallel heat fluxes vary significantly during the first EDA phase (EDA 1), yet by all measures the width of the footprint remains unchanged. In contrast, a step change in the footprint width is seen in the transition from EDA 1 to EDA 2. Pedestal and SOL electron pressure profiles (averaged over the times indicated by red and blue bars in online color version) are correspondingly different (bottom panel), with the "reduced pedestal height" of the EDA 2 phase displaying a flatter pressure profile in the SOL.

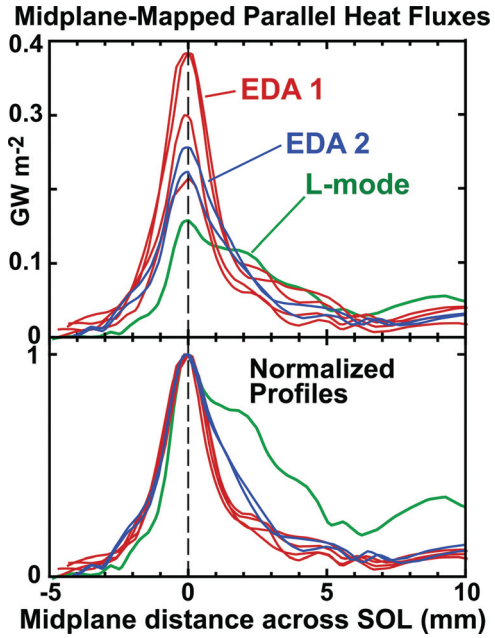

FIG. 5. (Color online) Divertor parallel heat flux profiles at multiple time points from the discharge shown in Fig. 4. Despite the variation in peak parallel heat flux, normalized heat flux profiles during the first EDA phase are identical. Profiles from the EDA 2 phase are also invariant in time, but are distinctly broadened relative to those from EDA 1.

separate EDA phases (EDA 1 and EDA 2), with a clear quasicoherent mode present in both. The first EDA phase (EDA 1) begins with the initial ramp-up in ICRF power: plasma density slowly rises and intrinsic impurities (molybdenum, boron) accumulate, as indicated by the increasing P_{RAD}. In response, plasma thermal energy peaks and then droops with an associated variation in P_{SOL}. The net result is a 50% variation in peak $q_{//}$ arriving at the outer divertor. Yet, by all three measures, the width of the heat flux profile is found to be invariant during this phase.

During the second EDA phase (EDA 2), line-averaged density falls slightly and impurity accumulation is arrested. It is interesting that the heat flux widths are markedly different in this phase compared to EDA 1: integral λ_q step up from 4 mm (EDA 1) to 5 mm (EDA 2) and e-folding widths increase by a factor of $\sim$2. This is perhaps associated with the enhanced level of particle transport across the pedestal that supports the density/impurity pump-out behavior. In any case, the step change in heat flux widths cannot be simply ascribed to changes in P_{SOL} since it is only slightly different between the two phases. Further detail can be gleaned from snapshots of the time-evolving parallel heat flux profiles shown in Fig. 5. While a clear variation in power flow is seen (top panel), normalized profiles are invariant within each phase (bottom panel). Thus, it is clear that the level of power flow into the scrape-off layer does not influence the width of the heat flux footprint. Regression analysis of the full set of EDA H-mode discharges leads to the same conclusion:[17] λ_q is statistically independent of P_{SOL}.

It is interesting that the heat flux widths are associated with the phase of the discharge (L-mode, EDA 1, EDA 2) rather than the magnitude of the boundary layer heat flow. They appear to be directly associated with the edge transport barrier, upon which the pedestal and discharge performances depend. As shown in the bottom panel of Fig. 4, the pedestal height attained during EDA 2 was significantly lower than in EDA 1. Associated with EDA 2 is a flattened SOL pressure profile, directly correlating with the larger heat flux widths. As we will see below, this connection is born out in the statistics of many discharges: plasmas that manage to attain high stored energy tend to have narrow heat flux widths. This behavior in C-Mod has been seen before in the main plasma SOL—as confinement improves, SOL pressure gradient scale lengths tend to become shorter.[29] It should be noted that ASDEX-Upgrade has examined similar relationships, producing an explicit power-law scaling of heat flux widths in terms of H-mode confinement factor.[4] Thus, one must look to the physics of the edge transport barrier as controlling the width of the power channel in the SOL.

C. Connection to upstream profiles: $T_e^{7/2}$ and nT_e mappings

Under attached divertor conditions, we expect that heat flux footprint should reflect in some way the conditions measured upstream at the outer midplane. Since electron conduction typically dominates heat flow along field lines, it is often assumed that the heat flux channel width λ_q should map to $2\lambda_{Te}/7$, i.e., a small fraction of the electron temperature e-folding width. This relationship follows from the Spitzer–Harm expression[30] for parallel electron heat conduction in a collisional plasma fluid, $q_{//e,\mathrm{fluid}} = -\frac{2}{7}\kappa_0 \nabla_{//} T_e^{7/2}$. For the case of uniform heat deposition into a flux tube of length L that connects from midplane to divertor, a simple estimate for the parallel heat flux arriving at the surface is $q_{//,\mathrm{fluid}} \approx \frac{4}{7}\kappa_0 (T_{e,\mathrm{mid}}^{7/2}/L)$, provided that $T_{\mathrm{e,mid}} \geq \sim 1.5 T_{e,\mathrm{div}}$.

Figure 6 shows $q_{//,\mathrm{fluid}}$ deduced from a typical Thomson scattering T_e profile compared with $q_{//}$ measured at the divertor target. It is clear that this $T_e^{7/2}$ "rule-of-thumb" does not apply: $q_{//,\mathrm{fluid}}$ decays too rapidly and yields a peak heat flux that is much higher than observed, even allowing for relative shifts due to field line mapping errors. (Note: one cannot shift the profiles by an arbitrary amount since the total power arriving at the divertor, i.e., the area under the curves, must roughly agree.) Physical processes neglected in this formulation must account for this discrepancy. These include kinetic corrections[31,32] (which must be included in these plasmas since the collisional mean-free paths for electrons are a significant fraction of L), cross-field transport that can spread the footprint via collisional or turbulence processes[33,34] or via stochastic magnetic field lines in the vicinity of the x-point (e.g., Ref. 35) and non-negligible radiation in the divertor (photons plus charge exchange). A better correspondence between the divertor heat flux profile and midplane plasma conditions is found simply from the requirement that the electron pressure should map along field lines. Assuming the electron pressure at the divertor target is approximately equal to half the upstream value, the parallel heat flux at the target can be computed from standard sheath formulations,[36] using the measured divertor T_e to evaluate the local sound speed, $q_{//,\mathrm{sheath}} \approx 0.5\,\gamma_{sh}(nT_e)_{\mathrm{mid}} C_{s,\mathrm{div}}$. Figure 6 shows $q_{//,\mathrm{sheath}}$ deduced from this method, with

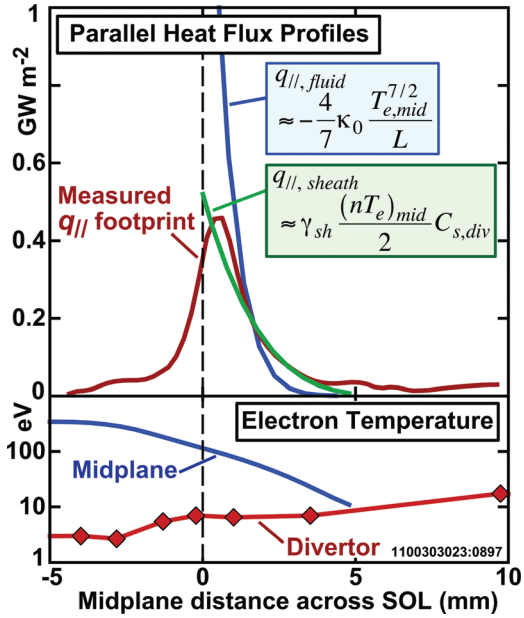

FIG. 6. (Color online) A typical parallel heat flux profile in the divertor is compared with two different estimates of that quantity based on "midplane" temperature and density profiles. Data from C-Mod's edge Thomson scattering diagnostic are used for this purpose (top panel). The overall width and magnitude of the heat flux footprint is best described by a model that simply maps the midplane pressure profile to the divertor plate and accounts for the parallel heat flux through the sheath using T_e values measured at the divertor to evaluate the local sound speed ($q_{//,\mathrm{sheath}}$). The "two-point model" estimate of the parallel heat flux profile ($q_{//,\mathrm{fluid}}$), i.e., Spitzer–Harm electron parallel conduction (without corrections associated with kinetic effects, cross-field heat spreading or volumetric losses), clearly does not apply—it incorrectly estimates both the peak heat flux and the decay length that is observed. Electron temperature profiles at the "midplane" and divertor locations are shown in the bottom panel.

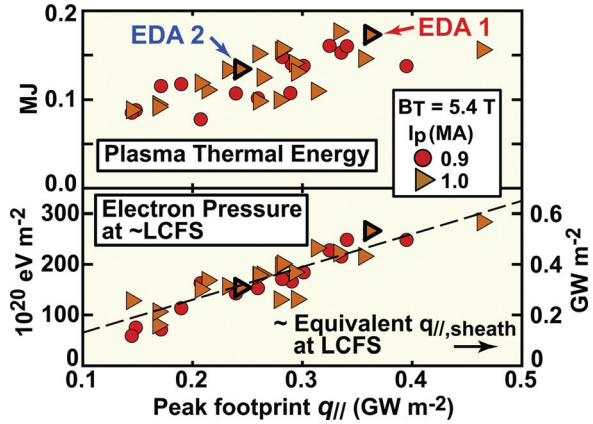

FIG. 7. (Color online) A separatrix-finding algorithm is employed, which assumes that the divertor heat flux profile matches the shape of the upstream electron pressure profile. As a consistency check, the electron pressures at the last-closed flux surface, along with their corresponding pressure-mapped sheath heat fluxes, are compared to peak parallel heat fluxes arriving at the divertor plate (bottom panel). An approximately linear relationship is found, accommodating discharges with significant variation in heat flux widths, such as those seen in the EDA 1 and EDA 2 time slices of Fig. 4. Plasma thermal energy is also correlated with peak divertor heat flux (top panel), consistent with plasma pressure at the boundary being the common element.

$\gamma_{sh} = 7$. Since the electron temperature profile across the divertor target tends to be flat, $q_{//,\mathrm{sheath}}$ is essentially proportional to the upstream electron pressure profile. This profile shape is found to be similar to the observed heat profile in the common flux region.

Adopting $q_{//,\mathrm{sheath}}$ as the correct mapping formula, it is possible to use this as a separatrix-finding algorithm to compensate for shot-to-shot variation in the flux surface mappings of the upstream Thomson scattering data. This is analogous to the way the Spitzer–Harm expression has been employed in the past.[6] Here we explore the consequences of aligning the upstream n_e,T_e profiles by this method. The integrated heat flux from $q_{//,\mathrm{sheath}}$ is forced to be equal to $\frac{1}{2}$ of the total heat flux arriving at the divertor, as inferred from IR measurements. The factor of $\frac{1}{2}$ is used as a rough approximation to account for two inadequacies in the data set: (1) the Thomson scattering data does not extend into the far SOL region where a tail is observed in the heat flux profile (Fig. 3), and (2) it is unclear how much of the divertor heat flux profile should be included on the "left" side of its peak, since electron pressure does not map along field lines from the midplane into the private flux zone. Divertor T_e profiles are taken to be flat with $T_e = 10$ eV. The flux surface mapping adjustments from this procedure are found to be small relative to the application of the Spitzer–Harm constraint, typically 1 mm or less. Figure 7 examines the resulting relationship that is obtained between electron pressures at the LCFS and the peak parallel heat fluxes measured on the outer divertor for all the 0.9 and 1.0 MA discharges in the EDA H-mode data set (5.4 T). An approximately linear relationship is found, consistent with the mapping algorithm employed and the idea that the upstream electron pressure profile and divertor heat flux profile shapes roughly correspond, even as the heat flux widths vary among discharges (see EDA 1 and EDA 2 data points marked). More reassuring, perhaps, is the observed relationship between plasma thermal energy and peak heat flux footprint that is also shown in Fig. 7. These data are completely independent of the assumed mapping algorithm, yet they largely support the one employed here, i.e., plasma thermal energy and peak heat flux on the divertor are seen to be roughly proportional, with plasma pressure at the LCFS being the common element that connects between the two.

D. Heat flux width scalings

Examining the full range of currents and fields explored for EDA H-modes, we find that the connection between achievable plasma thermal energy and heat flux footprint width, identified in Fig. 4, applies to all discharges. Plasma current is found to play an important role in this story as well. As illustrated in Fig. 8, heat flux widths generally decrease with increasing plasma thermal energy with no sensitivity to toroidal magnetic field strength. Higher plasma currents allow a higher thermal energy to be achieved, which in turn tends to be associated with a narrower heat flux footprint. For the discharges with the highest thermal energy per unit current, the e-folding decay length of the narrow power channel near the separatrix (see Fig. 3) exhibits an approximately $1/I_p$ scaling. No sensitivity to toroidal field strength is observed in this width parameter.

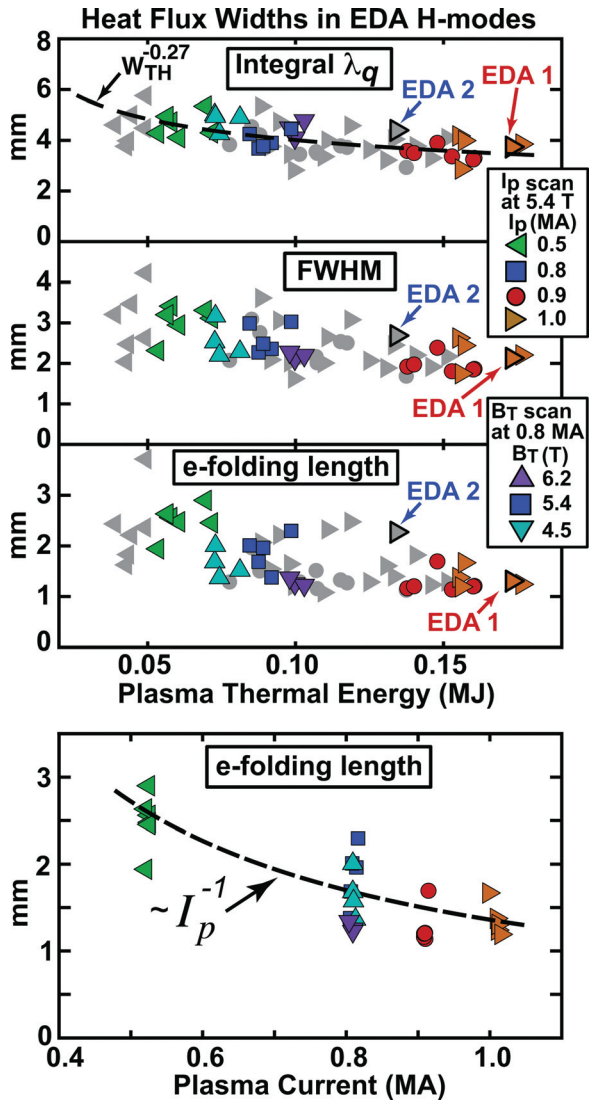

FIG. 8. (Color online) Heat flux footprint widths in EDA H-modes (as defined in Fig. 3) generally decrease with increasing plasma thermal energy, W_{TH}. The smallest widths therefore tend to occur at the highest currents (top panels). In discharges with the highest stored energy per unit current (colored symbols), the e-folding decay of the narrow heat-flux channel near the strike-point exhibits an approximately 1/*Ip* scaling, with no dependence on toroidal field (bottom panel). Symbols labeled EDA 1 and EDA 2 correspond to data from the two separate time intervals shown in Fig. 4.

E. Connection to H-modes in other tokamaks

In summary, we find that C-Mod's heat flux footprints in EDA H-mode are independent of power flow in the SOL, independent of toroidal field and exhibit a width that decreases with plasma thermal energy. The dominant influence is plasma current and the associated response of the transport barrier/H-mode pedestal, with the width of the upstream pressure profile setting the heat flux width. In the "best" EDA H-modes, i.e., discharges with the highest stored energy per unit current, the e-folding width of the narrow power channel near the separatrix scales approximately as $1/I_p$. These results are consistent with observations in DIII-D and NSTX ELMy H-modes, whether the data are averaged over ELMs or taken during ELM-free phases of the discharge.[8,37–39] Both machines report plasma current as the dominant scale parameter: widths scale as $1/I_p^{\alpha}$, with α in the range of 1–1.6; widths are found to be independent of toroidal field and power flow in the SOL. Heat flux footprint widths in DIII-D are also found to be much larger than the often-assumed $2\lambda_{Te}/7$ rule, being more on the order of λ_{Te}.[37]

IV. EFFECT OF MAGNETIC TOPOLOGY

The observation that λ_q is independent of toroidal field strength at fixed plasma current also means that λ_q is independent of q_{95}, or equivalently, field line connection length from good to bad curvature regions inside the LCFS, at fixed current. But, what about variations in field line length *outside* the LCFS? For example, simple transport arguments have been used to assert that cross-field decay lengths should scale according to connection length, $\lambda_q \sim L_{//}\sqrt{\chi_\perp/\chi_{//}}$, or square-root of connection length, $\lambda_q \sim \sqrt{L_{//}\chi_\perp/V_{th}}$, depending on parallel transport regime (diffusive versus free-streaming, respectively, e.g., Ref. 5). To help address this question, we studied the time evolution of heat flux footprints on the outer divertor in a number of discharges as the magnetic topology was changed dynamically from lower single-null (LSN) to double-null (DN) and slightly beyond.

A. X-point balance experiments

Representative results from a 1.1 MA ohmic L-mode plasma are shown in Fig. 9. The discharge begins in a LSN configuration. During this period, electron temperature profiles across the outer divertor target plate are measured via a small strike-point sweep. Electron temperature values there are under 30 eV, indicating a moderate recycling regime near the strike-point (parallel diffusive) and a sheath-limited regime further out into the SOL (parallel free-streaming). As indicated by the "magnetic x-pt balance" time trace, a rapid change in magnetic topology is initiated at 1.05 seconds, taking the plasma to a DN configuration at 1.125 s and into a slightly upper single-null configuration (USN) for a short period thereafter. Note that in going from LSN to DN, the total field line length in the SOL (divertor-to-divertor) is effectively cut in half, from 24 to 12 m in this case. Yet, the footprint width time traces show remarkably little response. Corresponding snapshots of heat flux footprints during this period are shown in the right panels of Fig. 9, with their horizontal axes shifted so as to align peak heat flux values. These profiles are found to be robustly resilient to the magnetic topology change. As one observes the location of the secondary separatrix (which marks the interface between 24 and 12 m field line length) dynamically sweep across the outer divertor, no evidence of a corresponding break-in-slope in any of the heat flux profiles is seen. Normalized outer divertor heat flux profiles essentially overlay, even for the nominal USN cases. For reference, a typical profile, highlighted in black in Fig. 9, is artificially narrowed by a factor of 2 and $\sqrt{2}$ (see respective blue and red profiles in online color version). None of the measured profiles behave in this way. The same result has been observed for EDA H-mode discharges.[17]

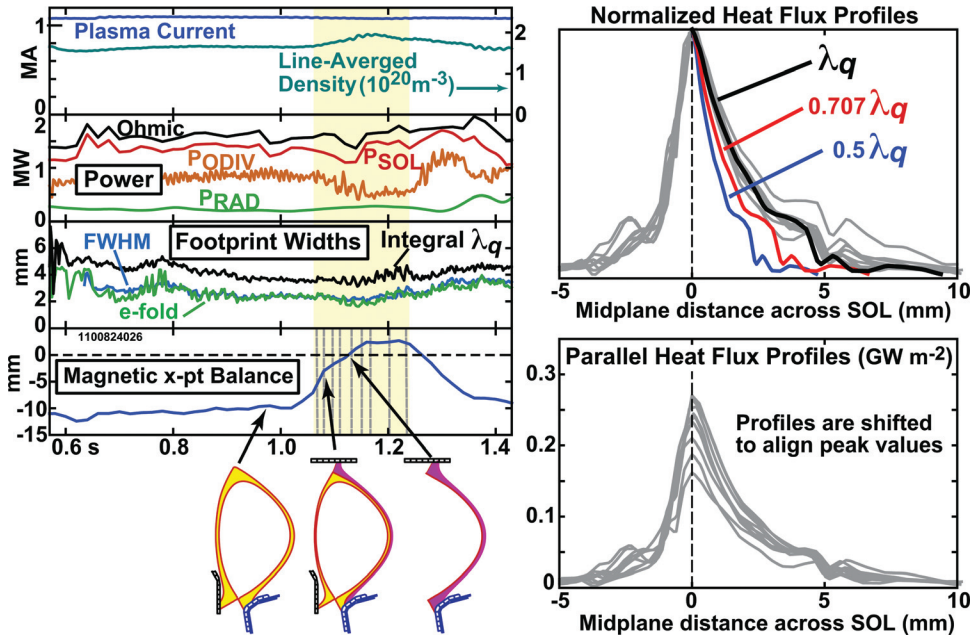

FIG. 9. (Color online) A sweep in magnetic topology from lower single-null (LSN) to double-null (DN) is performed in a 1.1 MA ohmic L-mode plasma (left panel). The time history of the x-point balance is shown in the lower left panel, which records the distance between the primary and secondary x-points mapped to the outboard midplane. Snapshots of outer divertor heat flux profiles over the time span of 1.07–1.25 s (indicated as dashed lines) are shown in the right panels. Despite the factor of 2 reduction in magnetic field line length to the divertor surfaces, the heat flux profiles are found to be remarkably resilient, exhibiting little or no change in cross-field decay length, even while the peak heat flux values decrease. For comparison, a typical profile is highlighted (black) and artificially narrowed by factors of 0.707 and 0.5 (red and blue lines overlayed in online color version).

B. Physics and implications

This result may seem puzzling at first but is consistent with previous C-Mod observations of scrape-off layer profiles in response to magnetic topology changes[22]—in changing from single to double-null, the electron pressure profiles in the low-field side SOL remained similar. It should be noted that two important field line lengths remained constant during these topology variation experiments: the field line length in the bad curvature region and the field line length from the outer midplane to the lower divertor. Thus, these data make sense if the heat flux profile on the outer divertor is rigidly set by a critical-gradient transport dynamic on the low-field side (e.g., interchange-driven turbulence). Whether the field line connects a long way around to the inner divertor (single-null) or a short way to the upper divertor (double-null) is apparently not of primary importance.

This transport phenomenology is important to keep in mind when assessing the relative benefits of various magnetic topologies for a reactor. Our data indicate that despite the associated factor of two reduction in field line length in going from LSN to DN, the heat flux widths do not get narrower. This is good news. On the other hand, the data also suggest that the extended field line length of advanced divertor topologies[40,41] will not by itself spread the heat flux footprint width (as mapped to the outer midplane) beyond that which is set by the intrinsic SOL transport dynamics. Thus, the true advantage of these techniques will likely come from their increase in magnetic flux expansion (to spread the heat flux over a larger divertor target area) and their increase in divertor volume (to dissipate parallel heat fluxes via radiation and charge–exchange losses).

V. OHMIC L-MODE PLASMAS

The final subject of our experimental investigation is ohmic L-modes. Ohmic L-modes are particularly valuable for boundary layer research because they can be studied over a large parameter range and investigated in detail with C-Mod's extensive array of edge diagnostics. We targeted plasmas over a wide range of plasma currents ($I_p = 0.55$, 0.8, 1.1, 1.2 MA) and toroidal magnetic fields ($B_T = 4$, 5.4, 8 T), with normalized plasma densities varied over the range $0.1 < \bar{n}_e/n_G < 0.4$. The principal tools for divertor heat flux investigation were the embedded sensors (Fig. 1): divertor Langmuir probes, cross-checked against surface thermocouples. Conditions upstream near the outer midplane were recorded with a scanning Langmuir probe.

Divertor profiles were examined with high resolution by performing slow strike-point sweeps across the divertor under otherwise constant conditions. In low-to-moderate divertor recycling regimes ($0.1 < \bar{n}_e/n_G < 0.25$), parallel heat flux profiles obtained from surface thermocouples and divertor Langmuir probes were found to closely match the standard sheath heat flux formulation, $q_{//,\text{sheath}} = \gamma_{sh} T_e J_s$. Here J_s is the parallel ion saturation current density, with the value, $\gamma_{sh} = 7$, found to be reasonable. However, as the divertor transitions into a high-recycling regime, the Langmuir probe data are found to substantially over-estimate the parallel heat fluxes relative to the surface thermocouples. This remarkable result appears to be closely related to the "death ray" phenomenon reported early in C-Mod's operation[42] where the divertor Langmuir probes would report a local, factor of ~2 over-pressure relative to values measured upstream in the SOL. This observation is important; it clearly indicates that the "death ray" phenomenon is an artifact that is specific to Langmuir probe operation and that the probe data must therefore be interpreted differently in this regime—a topic that is presently under investigation.[28] In recognition of this fact, we restrict our attention here to divertor Langmuir probe data in the density range $0.1 < \bar{n}_e/n_G < 0.25$, while midplane scanning probe data are examined over the full density range. It should be noted that because of this

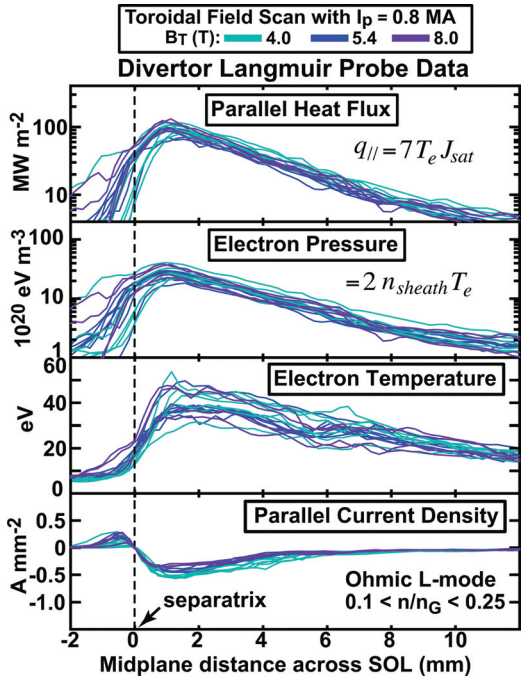

FIG. 10. (Color online) Divertor plasma profiles recorded by embedded Langmuir probes during ohmic L-mode, strike-point sweep experiments. To align the profiles, the separatrix location is taken to be the point where the parallel current density to the divertor surface crosses zero (bottom panel). The parallel heat flux density to the surface is estimated from standard sheath theory, with a heat transmission factor of 7. Despite the factor of two change in toroidal field at fixed current, the electron pressure and parallel heat flux profiles are virtually identical, both in magnitude and in decay length across the scrape-off layer.

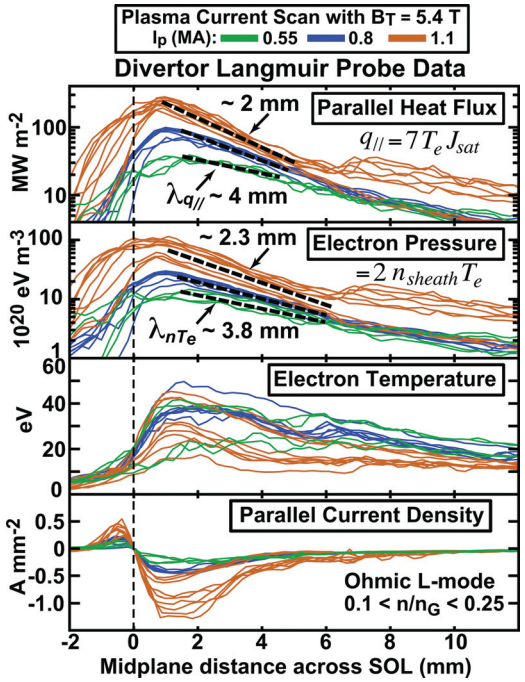

FIG. 11. (Color online) Divertor plasma profiles from ohmic L-mode discharges with fixed toroidal field and different plasma currents (data processing identical to that of Fig. 10). Peak plasma pressures and parallel heat fluxes rise with current, as expected for $n_e/n_G \sim$ constant in ohmic plasmas. More significantly, cross-field decay lengths are found to decrease with increasing plasma current over the region of 2–5 mm from the separatrix. (Note: the "shoulder" in the pressure and heat flux profiles for the 1.1 MA that extends beyond 7 mm is caused by plasma conditions changing during the final portion of the strike-point sweep.)

restriction on $\bar{n}_e/n_G$, we are not able to examine high-recycling divertor cases in the L-mode dataset, i.e., discharges in which the divertor electron temperature profile becomes flat or exhibits its characteristic profile inversion (colder near the strike-point), similar to what is seen in the EDA H-modes discussed in Sec. III (see Fig. 6).

A. Divertor heat flux and pressure profiles

Figures 10 and 11 show divertor target profiles obtained from the embedded Langmuir probe array: net parallel current density arriving at the plate ($J_{//}$), electron temperature (T_e), presheath electron pressure ($2n_{\text{sheath}}T_e$), and parallel heat flux ($q_{//} = 7\,T_e\,J_{\text{sat}}$). The profiles shown in Figs. 10 and 11 are composites. Data from adjacent probes partially overlap in flux surface coordinate due to the strike-point sweep. The average values are therefore shown.

In order to correct for offsets in flux surface mappings, which can vary on a shot-to-shot basis as plasma current and/or toroidal magnetic field is changed, the $J_{//}$ data are used as a reference marker. We define the separatrix location (zero coordinate) to be the location where $J_{//}$ goes to zero; all profiles are shifted as needed to meet this condition. The physics justification for this treatment comes from the observation that $J_{//}$ is composed primarily of two parts: a thermoelectric component[42] and a Pfirsch–Schluter component that changes sign across the strike-point.[43] Note that once this adjustment is done there is no "wiggle room" left in shifting the profiles with respect to one another.

Bearing this in mind, the data in Fig. 10 show a remarkable result. Despite the factor of 2 change in toroidal field, the parallel heat flux profiles and electron pressure profiles are found to be virtually identical, both in magnitude and decay length. Moreover, this correspondence is not restricted to the near SOL region; it extends out 10 mm or more. This result offers an important clue about the underlying transport dynamics. One possibility is that the factor of 2 increase in parallel connection length is directly compensated by the associated factor of 2 increase in toroidal field strength. It should be noted that such a behavior is consistent with interchange-driven turbulence in a toroidal system in which Alfven waves propagate along the magnetic field in response to the curvature drive:[44] Since the Alfven wave speed is proportional to magnetic field strength, its transit time in the poloidal direction from bad to good curvature regions is largely unaffected by variation in toroidal magnetic field strength at fixed plasma current. As we will see below, this observation is particularly relevant because it makes contact with the more general tendency for the edge plasma to hold the MHD ballooning parameter, α_{mhd}, roughly invariant at fixed parallel collisionality. In this context, α_{mhd} is simply a measure of the relative strength of ideal interchange growth rate versus shear Alfven wave damping; it is independent of toroidal field strength at fixed current.

Turning to Fig. 11, we see how plasma profiles respond to a factor of 2 increase in plasma current at fixed toroidal field (and fixed $\bar{n}_e/n_G$). The electron pressure and parallel

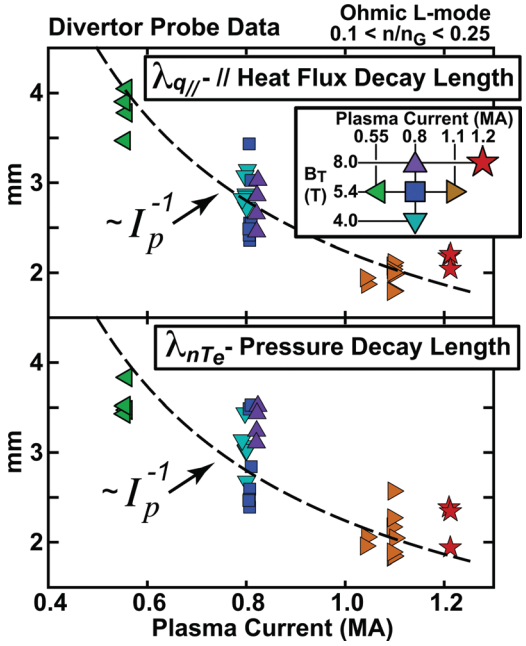

FIG. 12. (Color online) Parallel heat flux and pressure decay lengths at the divertor target plate for a series of ohmic L-mode plasmas in which the strike-point was swept across embedded Langmuir probes. The e-folding lengths are evaluated at the location of 4 mm into the SOL, mapped to the outer midplane (see coordinate axis in Fig. 10). The e-folding lengths are found to scale approximately as $1/I_p$ for this range of normalized central plasma densities ($0.1 < \bar{n}_e/n_G < 0.25$).

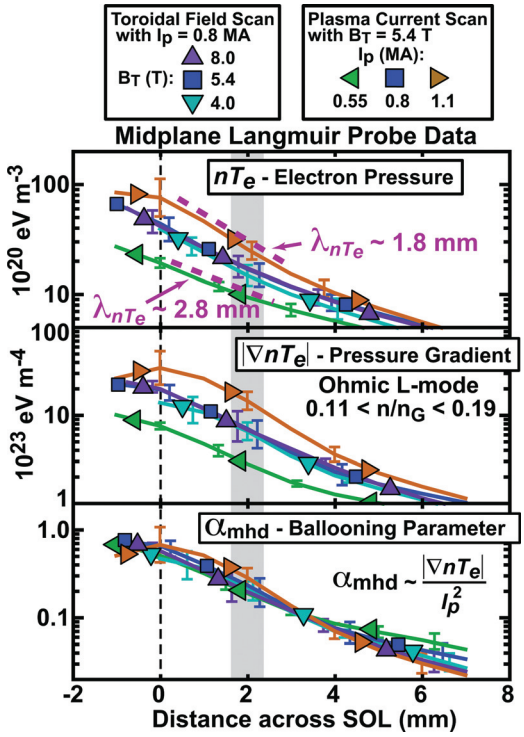

FIG. 13. (Color online) Information on midplane electron pressure profiles obtained from multiple plunges of a scanning Langmuir probe. Discharge conditions correspond to those presented in Figs. 10–12. Approximately five probe scans are performed for each condition; average profiles with corresponding 1-sigma statistical error bars shown. The behavior of the SOL pressure profiles is consistent in detail with the response seen at the divertor plate: a factor of 2 increase in toroidal field at fixed current produces no change, while pressure profiles (top panel) and pressure gradients (middle panel) increase with plasma current. Also pressure gradient scale lengths tend to decrease with increasing current (top panel). As noted in previous studies (Refs. 9, 10), there is an overall tendency for pressure gradients near the last-closed flux surface to be "clamped" at a fixed value of the MHD ballooning parameter, regardless of engineering parameters (bottom panel). Conditions at the 2 mm location (gray band) are explored in Fig. 14 over a wider range in $\bar{n}_e/n_G$.

heat flux profiles show an overall increase, as expected. However, the gradient scale lengths of pressure (λ_{nTe}) and parallel heat flux ($\lambda_{q_{//}}$) are reduced as current is increased. Figure 12 examines this behavior in more detail. An approximately $1/I_p$ dependence of $\lambda_{q_{//}}$ and λ_{nTe} is found. This result is interesting; it makes contact with the $\sim 1/I_p$ scaling seen in the e-folding lengths of EDA H-modes (Sec. III), despite the fact that the plasmas are in completely different confinement regimes.

B. Upstream pressure profiles and normalized gradients

Figure 13 shows the corresponding behavior of upstream plasma conditions: electron pressure profiles (nT_e), their gradients ($|\nabla nT_e|$), and their normalized gradients (α_{mhd}). α_{mhd} is the MHD ballooning parameter evaluated as $\alpha_{\mathrm{mhd}} = 4\,\mu_0\, q_{95}^2\, R\, |\nabla nT_e|/B^2$ in MKS units. It is important to note that the parametric responses seen here are virtually identical to those observed at the outer divertor target: Electron pressure profiles are robustly insensitive to a factor of 2 change in toroidal magnetic field at fixed current. When plasma current is doubled at fixed $\bar{n}_e/n_G$, plasma pressure increases and pressure gradient scale lengths in the near SOL become shorter.

Particularly interesting is the response of the normalized pressure gradients. At fixed plasma current, α_{mhd} is robustly invariant to changes in magnetic field, a simple consequence of the electron pressure profiles being unchanged. But when plasma current is doubled, pressure gradients roughly quadruple. This response is just what is needed to hold α_{mhd} roughly fixed—another remarkable behavior.

In order to explore these trends more fully, values of α_{mhd} and λ_{nTe} at the outer midplane were measured and tracked for the entire set of ohmic L-mode discharges created for the study. Figure 14 shows the result. These quantities are evaluated at a location 2 mm outside the LCFS and plotted versus $\bar{n}_e/n_G$. Also shown on the abscissa are approximate values of parallel collisionality, $\nu^*_{//} = \pi R\, q_{95}/\lambda_{ei}$. Here λ_{ei} is the electron-ion mean free path evaluated from midplane parameters (2 mm location). These data reveal that the $\sim 1/I_p$ scaling of λ_{nTe} is restricted to low collisionality regimes where the divertor is in a low-recycling or sheath-limited state. As collisionality is raised and the plasma enters into a high recycling regime, this scaling is at first diminished and then lost. In particular, λ_{nTe} in the low current plasmas (0.55 MA) become smaller while λ_{nTe} in the high current plasmas (1.1, 1.2 MA) become larger. Just prior to the onset of divertor pressure loss and associated detachment physics, λ_{nTe} are statistically indistinguishable, hovering around ~2.3 mm. Since our experimental program was restricted to attached regimes, we did not track the behavior beyond this point.

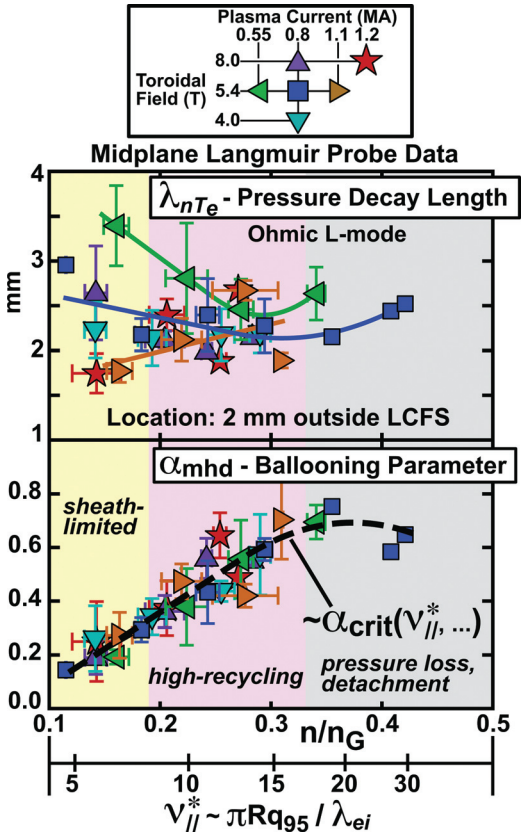

FIG. 14. (Color online) Upstream electron pressure decay lengths (top panel) and MHD ballooning parameter (bottom panel) at a location 2 mm outside the last-closed flux surface, tracked as a function of normalized discharge density, $\bar{n}_e/n_G$. The approximate value of miplane parallel collisionality, $\nu^*_{//}$, evaluated at the 2 mm location, is also shown. The corresponding divertor state is noted. The data points represent average values from a number of probe scans; error bars indicate typical ±1 standard deviation in the data sample. Smooth curves shown in the top panel are spline fits to the full set of data points. The strong $\sim 1/Ip$ dependence of pressure decay length at low collisionality is found to diminish as the collisionality is raised. Nevertheless, normalized pressure gradients (α_{mhd}) tend to cluster around a value of this quantity, α_{crit}, which appears to be predominantly a function of parallel collisionality and is statistically independent of plasma current and toroidal field.

C. Connections to marginal stability transport paradigm

Perhaps the most important observation that has come out of the ohmic L-mode data set is the behavior seen in the bottom panel of Fig. 14. Despite the factor of 2 variation in current and field, the boundary layer plasma organizes itself in such a way as to keep α_{mhd} approximately invariant for a fixed value of parallel collisionality. This behavior has been noted before[9] and tested for its sensitivity to magnetic topology and associated edge plasma flow conditions.[10] The data presented here separately verify the result and extend the observation to a larger range of fields and currents. In addition, the measurements at the divertor plate (Figs. 10 and 11), independently confirm this plasma response and show that it is directly connected to the scaling of the divertor heat flux footprints observed in the attached plasma regimes.

The tendency for the plasma to organize itself in this way is broadly consistent with models for electromagnetic fluid drift turbulence[45–49] which, among other things, identify α_{mhd} and plasma collisionality as key parameters that control the level of turbulence and transport in the boundary layer. The overall idea is that transport in the vicinity of the LCFS increases sharply when α_{mhd} exceeds a threshold value, α_{crit}, and that this critical value has a strong dependence on parallel collisionality, $\alpha_{crit}(\nu^*_{//}, \ldots)$. As a consequence of the critical-gradient dynamic, plasma intermittently "spills" onto the open field lines of the SOL where flute-like instabilities take over: curvature drift causes a dipole-like polarization of the resulting plasma "blobs," leading to a rapid $E \times B$ convection outward in major radius on the low-field side.[50–52] Thus the parametric dependence of α_{crit} is the key physics component since it sets the boundary layer profiles; α_{mhd} tends to be "clamped" at that value. This overall picture is consistent with the heat flux footprint observations, which identify plasma current as the dominant external control parameter and magnetic x-point topology (LSN versus DN) as relatively insignificant.

It should be pointed out that the collisionality dependence of α_{crit} shown in Fig. 14 is slightly different than what was identified in earlier work.[10] The previous study found the dimensionless ratio $q_{95}^2 R/\lambda_{ei}$ as providing good alignment of the data in the two-dimensional phase-space (α_{mhd}, collisionality), while the new data suggest that the relevant dimensionless grouping is simply $q_{95}R/\lambda_{ei}$, i.e., the parallel collisionality shown in Fig. 14. The reasons for this difference are unknown at the present time. However, the new data in Fig. 14 were taken over a wider range of q_{95}, which should provide a more stringent test of the collisionality normalization. In addition, the data quality from the horizontal scanning probe has since been improved with installation of advanced probe head geometries and upgraded data acquisition systems.

Clearly, more work needs to be done on both the experimental and theoretical fronts to fully explain the relationships uncovered here, including the $\sim 1/I_p$ scaling of λ_{nTe} that appears at low collisionality. The results reported in this paper are just a part of the ongoing experimental effort that is aimed at unfolding this physics.

VI. SUMMARY

An extensive array of divertor heat flux instrumentation was recently installed in Alcator C-Mod with the aim of improving the understanding of boundary layer heat transport. Over the past year, a series of dedicated experiments were performed to map out the parametric dependences of divertor heat flux footprints (peak $q_{//}$, λ_q) over a wide range of engineering parameters (toroidal field, plasma current, input power, density) and to examine their relationships to plasma conditions in the boundary layer and core. Three separate experimental investigations were performed: (1) EDA H-modes, (2) plasmas with dynamically varied magnetic x-point topology, and (3) ohmic L-modes, all under attached divertor conditions so as to provide a clear measure of the power exhaust channel.

C-Mod's heat flux footprints in EDA H-modes are found to exhibit a two zone structure: a narrow power channel near the separatrix of ~2 mm wide and a tail that extends into the

far SOL region. Contrary to some empirical scaling laws, footprint widths are found to be independent of power flow in the SOL. In time-evolving EDA H-modes, peak $q_{//}$ values exhibit 50% or more variation while the profile shapes remain identical. Instead, footprint widths are connected to the edge transport barrier, making step changes as the plasma transitions from different confinement regimes: L-mode, EDA H-mode with impurities accumulating and EDA H-mode with impurity accumulation arrested. Thus the performance of the discharge, as measured by the plasma thermal energy and the development of a strong pedestal, is closely associated with the formation of a narrow power channel width. This behavior is reflected in the statistics of many discharges—plasmas that manage to attain high thermal energy content tend to have narrow heat flux widths. Plasma current plays a key role in this story since it sets the upper bound on pedestal pressure/thermal stored energy. Plasmas with the highest thermal stored energy per unit current exhibit a power e-folding width near the strike-point that scales roughly as $1/I_p$. No dependence on toroidal magnetic field strength is found. These results are consistent with heat flux width scalings reported from NSTX and DIII-D for ELMy H-mode regimes[8] (independent of field, independent of power in the SOL and scaling as $\sim 1/I_p^{\alpha}$ with $1 < \alpha < 1.6$), pointing to a common transport dynamic.

The overall width and magnitude of the heat flux footprint in EDA H-modes is found to be consistent with the upstream electron pressure profile. This relationship is expected since the electron temperature profiles at the divertor plate, $T_{e,\mathrm{div}}$, tend to be flat and parallel heat flux at the divertor sheath is roughly proportional to pressure, $(nT_e)_{\mathrm{div}} \sim 0.5(nT)_{e,\mathrm{mid}}$, times the square-root of $T_{e,\mathrm{div}}$. In contrast, a commonly used "rule-of-thumb" that estimates the heat flux footprint based on Spitzer–Harm parallel electron conduction, $q_{//,\mathrm{fluid}} \propto T_{e,\mathrm{mid}}^{7/2}$, clearly does not apply; it incorrectly estimates both the peak heat flux and the decay length that is observed.

The influence of total magnetic connection length in the SOL on heat flux footprint shape is examined in discharges where the magnetic topology is changed dynamically from lower single-null to double-null under otherwise identical conditions. Heat flux footprints are found to be robustly insensitive to total magnetic field line length, consistent with the idea that interchange-driven transport in the low-field portion of the SOL primarily sets the profile shape. This result is good news for tokamak operation with a double-null configuration since the heat flux widths do not narrow relative to the single-null case.

Finally, ohmic L-mode discharges are examined over a wide range of plasma currents and toroidal fields. Strike-point sweeps are used to map out divertor heat flux and electron pressure profiles across the outer target with high spatial resolution; scanning probes are used to record the corresponding conditions upstream in the SOL. Despite a factor of 2 change in toroidal field strength, divertor heat flux and electron pressure profile shapes are found to be robustly invariant at fixed plasma current. It is noted that this result is consistent with expectations from ideal interchange-driven turbulence, in which the poloidal transit time of shear Alvfen waves is unaffected by the toroidal field at fixed current. Also consistent with this picture, plasma current is found to strongly affect heat flux footprints and divertor electron pressure profiles. Under low collisionality conditions ($\bar{n}_e/n_G < 0.2$), heat flux e-folding lengths in the near SOL region scale as $\sim 1/I_p$, which makes contact with the behavior seen in EDA H-modes. This trend is reflected in the upstream plasma profiles as well; electron pressure e-folding lengths scale as $\sim 1/I_p$ in this collisionality range. Yet, as the divertor transitions into a high-recycling regime, the pressure gradient scale lengths (λ_{nT_e}) loose their sensitivity to I_p, tending toward a value that is independent of I_p.

More tellingly perhaps is the behavior of the upstream electron pressure profiles (nT_e) and their gradients ($|\nabla nT_e|$). As plasma current is doubled at fixed collisionality, these quantities approximately quadruple. Normalized upstream electron pressure gradients, $\alpha_{\mathrm{mhd}} \propto |\nabla nT_e|/I_p^2$, remain approximately invariant at fixed collisionality. This remarkable result, which persists over the full range of currents/fields studied, is consistent with previous investigations[9,10] and extends the observation to a wider range of currents and fields. Moreover, the present study establishes clear connections between the parametric dependences of this boundary layer transport phenomenology and the observed scalings of the divertor heat flux footprint—they are essentially the same.

Taken together, the picture of boundary layer heat transport that emerges for ohmic L-mode discharges is one in which pressure profiles (which roughly determine the heat flux profiles) are largely set by critical-gradient dynamics: transport in the vicinity of the LCFS increases sharply when α_{mhd} exceeds a critical value, α_{crit}; α_{crit} in turn has a strong dependence on parallel collisionality, $\alpha_{\mathrm{crit}}(\nu^*_{//}, \ldots)$. The fact that there effectively exists a α_{crit} in the boundary layer and that it can be parameterized primarily as a function of collisionality is a key finding. These observations call for further experimental and theoretical investigation.

It should be noted that a critical α_{mhd} paradigm is proving quite successful in explaining the H-mode pressure pedestal width and height.[11] Our experimental observations suggest that a first-principles understanding of the power exhaust channel in a tokamak may come from similar insights.

ACKNOWLEDGMENTS

Alcator C-Mod's contributions to fusion energy science are made possible by the excellent engineers, technical staff, students, and scientists on the Alcator team. The FLIR SC7000 camera was supplied through C-Mod's collaboration with LANL, U.S. Department of Energy Award DE-AC52-06NA25396. This research is supported by U.S. Department of Energy Coop. Agreement DE-FC02-99ER54512.

[1]A. Loarte, in Proceedings of the 22nd IAEA Fusion Energy Conference; http://www-pub.iaea.org/MTCD/Meetings/FEC2008/it_p6-13.pdf, 2008.
[2]A. Loarte, B. Lipschultz, A. S. Kukushkin, G. F. Matthews, P. C. Stangeby, N. Asakura, G. F. Counsell, G. Federici, A. Kallenbach, K. Krieger, A. Mahdavi, V. Philipps, D. Reiter, J. Roth, J. Strachan, D. Whyte,

R. Doerner, T. Eich, W. Fundamenski, A. Herrmann, M. Fenstermacher, P. Ghendrih, M. Groth, A. Kirschner, S. Konoshima, B. LaBombard, P. Lang, A. W. Leonard, P. Monier-Garbet, R. Neu, H. Pacher, B. Pegourie, R. A. Pitts, S. Takamura, J. Terry, and E. Tsitrone, Nucl. Fusion 47, S203 (2007).
[3]F. Najmabadi, T. A. Team, A. Abdou, L. Bromberg, T. Brown, V. C. Chan, M. C. Chu, F. Dahlgren, L. El-Guebaly, P. Heitzenroeder, D. Henderson, H. E. St. John, C. E. Kessel, L. L. Lao, G. R. Longhurst, S. Malang, T. K. Mau, B. J. Merrill, R. L. Miller, E. Mogahed, R. L. Moore, T. Petrie, D. A. Petti, P. Politzer, A. R. Raffray, D. Steiner, I. Sviatoslavsky, P. Synder, G. M. Syaebler, A. D. Turnbull, M. S. Tillack, L. M. Waganer, X. Wang, P. West, and P. Wilson, Fusion Eng. Des. **80**, 3 (2006).
[4]A. Loarte, S. Bosch, A. Chankin, S. Clement, A. Herrmann, D. Hill, K. Itami, J. Lingertat, B. Lipschultz, K. McCormick, R. Monk, G. D. Porter, M. Shimada, and M. Sugihara, J. Nucl. Mater. **266**, 587 (1999).
[5]G. Kirnev, W. Fundamenski, and G. Corrigan, Plasma Phys. Controlled Fusion **49**, 689 (2007).
[6]A. Kallenbach, N. Asakura, A. Kirk, A. Korotkov, M. A. Mahdavi, D. Mossessian, and G. D. Porter, J. Nucl. Mater. **337**, 381 (2005).
[7]B. Lipschultz, X. Bonnin, G. Counsell, A. Kallenbach, A. Kukushkin, K. Krieger, A. Leonard, A. Loarte, R. Neu, R. A. Pitts, T. Rognlien, J. Roth, C. Skinner, J. L. Terry, E. Tsitrone, D. Whyte, S. Zweben, N. Asakura, D. Coster, R. Doerner, R. Dux, G. Federici, M. Fenstermacher, W. Fundamenski, P. Ghendrih, A. Herrmann, J. Hu, S. Krasheninnikov, G. Kirnev, A. Kreter, V. Kurnaev, B. LaBombard, S. Lisgo, T. Nakano, N. Ohno, H. D. Pacher, J. Paley, Y. Pan, G. Pautasso, V. Philipps, V. Rohde, D. Rudakov, P. Stangeby, S. Takamura, T. Tanabe, Y. Yang, and S. Zhu, Nucl. Fusion **47**, 1189 (2007).
[8]See http://www.science.doe.gov/ofes/ProgramTargets/FY2010_JRT_Q4report_final_withcover.pdf for USDoE (2010).
[9]B. LaBombard, J. W. Hughes, D. Mossessian, M. Greenwald, B. Lipschultz, and J. L. Terry, Nucl. Fusion **45**, 1658 (2005).
[10]B. LaBombard, J. W. Hughes, N. Smick, A. Graf, K. Marr, R. McDermott, M. Reinke, M. Greenwald, B. Lipschultz, J. L. Terry, D. G. Whyte, and S. J. Zweben, Phys. Plasmas **15**, 056106 (2008).
[11]P. B. Snyder, R. J. Groebner, A. W. Leonard, T. H. Osborne, and H. R. Wilson, Phys. Plasmas **16**, 056118 (2009).
[12]M. Sugihara and T. Takizuka, Plasma Phys. Controlled Fusion **44**, 299 (2002).
[13]R. J. Groebner and T. H. Osborne, Phys. Plasmas **5**, 1800 (1998).
[14]M. Greenwald, J. L. Terry, S. M. Wolfe, S. Ejima, M. G. Bell, S. M. Kaye, and G. H. Neilson, Nucl. Fusion **28**, 2199 (1988).
[15]B. LaBombard, J. L. Terry, J. W. Hughes, D. Brunner, J. Payne, M. Reinke, Y. Lin, and S. Wukitch, J. Nucl. Mater. (in press).
[16]J. L. Terry, B. LaBombard, D. Brunner, J. Payne, and G. A. Wurden, Rev. Sci. Instrum. **81**, 10E513 (2010).
[17]B. LaBombard, J. L. Terry, J. W. Hughes, D. Brunner, J. Payne, M. Reinke, I. Cziegler, S. Zweben, R. Granetz, M. Greenwald, I. Hutchinson, J. Irby, Y. Lin, B. Lipschultz, Y. Ma, E. S. Marmar, N. Mucic, W. Parkin, S. Pierson, R. Rosati, W. Rowan, H. Savelli, J. Stillerman, N. Tsujii, R. Vieira, G. Wallace, D. Whyte, S. Wolfe, S. Wukitch, G. Wurden, and J. Zaks, "Boundary Layer Heat Transport Experiments in Alcator C-Mod in Support of the FY2010 US DoE Joint Research Target," M.I.T. Plasma Science and Fusion Center Report PSFC/RR-10-14 report# PSFC/RR-10-14 (2010).
[18]R. J. Maqueda, G. A. Wurden, J. L. Terry, and J. A. Stillerman, Rev. Sci. Instrum. **70**, 734 (1999).
[19]J. L. Terry, B. LaBombard, D. Brunner, J. Payne, and G. A. Wurden, Rev. Sci. Instrum. **81**, 10E513 (2010).
[20]A. Hermann, in Proceedings of the 28th EPS Conference on Controlled Fusion and Plasma Physics (Madeira, Portugal, 2001).
[21]J. W. Hughes, D. Mossessian, K. Zhurovich, M. DeMaria, K. Jensen, and A. Hubbard, Rev. Sci. Instrum. **74**, 1667 (2003).
[22]B. LaBombard, J. E. Rice, A. E. Hubbard, J. W. Hughes, M. Greenwald, J. H. Irby, Y. Lin, B. Lipschultz, E. S. Marmar, N. Smick, S. M. Wolfe, and S. J. Wukitch, Nucl. Fusion **44**, 1047 (2004).
[23]N. Smick and B. LaBombard, Rev. Sci. Instrum. **80**, 023502 (2009).
[24]N. Smick, "Plasma flows in the Alcator C-Mod scrape-off layer," Ph.D. thesis, MIT, 2009.
[25]M. Greenwald, R. Boivin, P. Bonoli, R. Budny, C. Fiore, J. Goetz, R. Granetz, A. Hubbard, I. Hutchinson, J. Irby, B. LaBombard, Y. Lin, B. Lipschultz, E. Marmar, A. Mazurenko, D. Mossessian, T. Sunn Pedersen, C. S. Pitcher, M. Porkolab, J. Rice, W. Rowan, J. Snipes, G. Schilling, Y. Takase, J. Terry, S. Wolfe, J. Weaver, B. Welch, and S. Wukitch, Phys. Plasmas **6**, 1943 (1999).
[26]M. L. Reinke and I. Hutchinson, Rev. Sci. Instrum. **79**, 10F306 (2008).
[27]D. Brunner, B. LaBombard, J. Payne, and J. L. Terry, J. Nucl. Mater. (in press).
[28]D. Brunner, B. LaBombard, J. L. Terry, and M. Reinke, Bull. Am. Phys. Soc. http://meetings.aps.org/Meeting/DPP10/Event/131506 (2010).
[29]B. LaBombard, J. A. Goetz, I. Hutchinson, D. Jablonski, J. Kesner, C. Kurz, B. Lipschultz, G. M. McCracken, A. Niemczewski, J. Terry, A. Allen, R. L. Boivin, F. Bombarda, P. Bonoli, C. Christensen, C. Fiore, D. Garnier, S. Golovato, R. Granetz, M. Greenwald, S. Horne, A. Hubbard, J. Irby, D. Lo, D. Lumma, E. Marmar, M. May, A. Mazurenko, R. Nachtrieb, H. Ohkawa, P. O'Shea, M. Porkolab, J. Reardon, J. Rice, J. Rost, J. Schachter, J. Snipes, J. Sorci, P. Stek, Y. Takase, Y. Wang, R. Watterson, J. Weaver, B. Welch, and S. Wolfe, "Transport studies in the scrape-off layer and divertor of alcator C-Mod," in *Plasma Physics and Controlled Fusion Research*, Montreal 1996 (IAEA, Vienna, 1997), Vol. 1, p. 825.
[30]L. Spitzer, Jr. and R. Harm, Phys. Rev. **89**, 977 (1953).
[31]P. C. Stangeby, J. M. Canik, and D. G. Whyte, Nucl. Fusion **50**, 125003 (2010).
[32]W. Fundamenski, Plasma Phys. Controlled Fusion **47**, 163 (2005).
[33]R. J. Goldston, Phys. Plasmas **17**, 012503 (2010).
[34]D. Hill, G. Porter, and T. D. Rognlien, J. Nucl. Mater. (in press).
[35]L. E. Sugiyama and H. R. Strauss, Phys. Plasmas **17**, 062505 (2010).
[36]P. C. Stangeby, Phys. Fluids **27**, 682 (1984).
[37]C. J. Lasnier, M. A. Makowski, J. A. Boedo, N. H. Brooks, D. N. Hill, A. W. Leonard, and J. G. Watkins, in Proceedings of the 23rd IAEA Fusion Energy Conference (IAEA, Daejon, Korea, 2010), pp. EXD/P3-20.
[38]C. J. Lasnier, M. A. Makowski, J. A. Boedo, S. L. Allen, N. H. Brooks, D. N. Hill, A. W. Leonard, J. G. Watkins, and W. P. West, J. Nucl. Mater. (in press).
[39]R. Maingi, C. E. Bush, R. Kaita, H. W. Kugel, A. L. Roquemore, S. F. Paul, V. A. Soukhanovskii, and N. Team, J. Nucl. Mater. **363**, 196 (2007).
[40]D. D. Ryutov, R. H. Cohen, T. D. Rognlien, and M. V. Umansky, Phys. Plasmas **15**, 092501 (2008).
[41]M. Kotschenreuther, P. M. Valanju, S. M. Mahajan, and J. C. Wiley, Phys. Plasmas **14**, 072502 (2007).
[42]B. LaBombard, J. A. Goetz, I. Hutchinson, D. Jablonski, J. Kesner, C. Kurz, B. Lipschultz, G. M. McCracken, A. Niemczewski, J. Terry, A. Allen, R. L. Boivin, F. Bombarda, P. Bonoli, C. Christensen, C. Fiore, D. Garnier, S. Golovato, R. Granetz, M. Greenwald, S. Horne, A. Hubbard, J. Irby, D. Lo, D. Lumma, E. Marmar, M. May, A. Mazurenko, R. Nachtrieb, H. Ohkawa, P. O'Shea, M. Porkolab, J. Reardon, J. Rice, J. Rost, J. Schachter, J. Snipes, J. Sorci, P. Stek, Y. Takase, Y. Wang, R. Watterson, J. Weaver, B. Welch, and S. Wolfe, J. Nucl. Mater. **241**, 149 (1997).
[43]M. J. Schaffer, A. V. Chankin, H. Y. Guo, G. F. Matthews, and R. Monk, Nucl. Fusion **37**, 83 (1997).
[44]B. D. Scott, "Low frequency fluid drift turbulence in magnetised plasmas," Max-Planck-Institut für Plasmaphysik Report# IPP 5/92 (2001).
[45]B. Scott, Plasma Phys. Controlled Fusion **39**, 1635 (1997).
[46]B. D. Scott, Plasma Phys. Controlled Fusion **49**, S25 (2007).
[47]B. N. Rogers and J. F. Drake, Phys. Rev. Lett. **79**, 229 (1997).
[48]B. N. Rogers, J. F. Drake, and A. Zeiler, Phys. Rev. Lett. **81**, 4396 (1998).
[49]B. D. Scott, Phys. Plasmas **12**, 062314 (2005).
[50]D.A. D'Ippolito, J. R. Myra, and S. I. Krasheninnikov, Phys. Plasmas **9**, 222 (2002).
[51]J. R. Myra, D. A. Russell, and D. A. D'Ippolito, Phys. Plasmas **13**, 112502 (2006).
[52]S. I. Krasheninnikov, D. A. D'Tppolito, and J. R. Myra, J. Plasma Phys. **74**, 679 (2008).